Active Disturbance Rejection Control Applied to a Three-Phase Grid-Connected Photovoltaic System

Ali BOUKHRISS
SAEDD, High School of Technology of Essaouira, Caddy Ayad University Morocco
a.boukhriss@uca.ma

***Abstract*—The objective of this work is to propose an active disturbance rejection control (ADRC) for a two-stage grid-connected photovoltaic (PV) array. ADRC combined with incremental conductance (ADRC_IncCond) is used to extract the maximum power from the PV array and compared to the fuzzy logic control (FLC) and the perturb and observe (P&O) algorithm. A two-stage inverter is also controlled by ADRC to keep the DC bus voltage constant and provide a unity power factor to the power supplied to the grid. The performance of the control is evaluated, under varying atmospheric conditions, by simulations in the Matlab Simulink environment.**

***Index Terms*—fuzzy logic control, maximum power tracking, photovoltaic system, reactive power control, voltage control.**

I. INTRODUCTION

The number of new renewable energy plants, namely wind and solar photovoltaic, is increasing worldwide. The global trend is to reduce the impact of polluting fossil fuels [1-2]. Despite their intermittent nature, the diversification of sites and the nature of the production process used: solar or wind, these production plants can participate in the secondary regulation of the network frequency, or even in the primary regulation, thanks to the reliability of current weather forecasts [3-4].

In this work, a grid-connected photovoltaic system is studied. Two configurations are widely used. The first one has a single stage, i.e. the PV panel is directly connected to the grid via an inverter [5-6], while the second one has an intermediate stage (DC/DC converter) between the PV panel and the inverter. The two-stage system keeps the DC bus voltage constant at the input of the inverter, thanks to the MPPT control of the boost converter [7].

The main objective is to inject the generated electrical energy into the electrical grid, guaranteeing a unit power factor, a minimum distortion rate and a maximum power extraction from the PV array. In this regard, DC/DC converter is controlled in MMPT mode to extract the maximum power from the PV. Several techniques are used in the literature. Perturb and observe technique P&O is widely used for its simplicity of implementation, but it exhibits oscillations around the maximum power point when environmental conditions change rapidly [8-10].

Incremental conductivity IncCond is also one of the most widely used MPPT techniques, overcoming some of the drawbacks of the P&O strategy. Many research studies have shown that IncCond outperforms P&O in terms of tracking efficiency, rise time, fall time and dynamic response [11-14].

In addition to conventional MPPT methods, soft computing techniques are increasingly used in PV systems, such as fuzzy logic control FLC, artificial neural network ANN, genetic algorithm GA etc.

FLC is very robust, it does not require accurate mathematical models. It has a fast response and less oscillation under changing atmospheric conditions [15-18]. However, it remains complex and its effectiveness depends on the performance of the designer and the accuracy of the rules.

Simulations show that the ANN variable step-size has a fast tracking speed, less oscillation and good efficiency compared to the fixed ANN step-size which has the same drawbacks as the P&O technique [19-20], nevertheless, it remains very complex and expensive and requires a lot of information on PV parameters.

In addition of the MPPT control, the inverter must be controlled. In the literature, PI controllers are widely used due to their simple design. However, they have limitations and weaknesses with respect to internal system disturbances.

To avoid problems related to non-linearities and internal disturbances in systems, non-linear control methods are widely used such as sliding mode control, back-stepping control etc. [21-22].

In this work, active disturbance rejection control ADRC will be applied. This technique allows real-time rejection of disturbances, whether internal or external, and does not require detailed knowledge of the mathematical model of the system. Its linear form (linear active disturbance rejection control LADRC) is simple in design and application for system control [23-25].

This technique will be applied to the control of the inverter in order to maintain a constant voltage at the DC bus and to ensure a unity power factor for the power fed into the grid. On the other hand, a combination of incremental conductance and active disturbance rejection control ADRC_IncCond will be used to control the DC/DC converter to ensure the maximum power point MPP from PV array.

The rest of this article is organized as follows. The design of the system structure is described in Section 2. In Section 3, the overview of the mathematical model of the system is presented. Section 4 describes the ADRC control technique. In Section 5, ADRC_IncCond, FLC and P&O techniques are applied to the first stage, while the ADRC is applied to the second stage. Simulations results are presented in Section 6 and finally a conclusion in Section 7.

Digital Object Identifier 10.4316/AECE.2022.01010

II. Design of the System Structure

The structure of the model considered consists of a two-stage PV system connected to the grid. The PV array is connected to a DC/DC converter controlled to track the maximum power point MPP. The grid is connected to the inverter via a filter and a DY transformer whose secondary winding (high voltage) is connected to the grid. A filter consisting of a resistor R_g in series with an inductor L_g is used to reduce harmonics generated by the use of power electronics semiconductors (IGBTs-Diodes). The PV system is based on a combination of modules providing 250 kW under standard test conditions (1000 W/m^2 and 25°C).

A 250 kW load is inserted between buses 1 and 2. Fig. 1 shows the schematic diagram of the model studied.

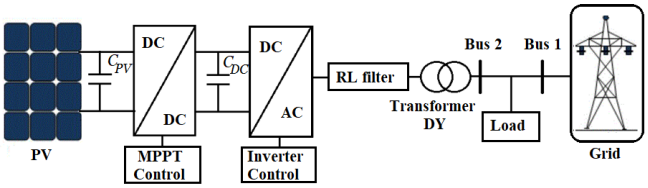

Figure 1. PV system schematic diagram

III. System Modeling

A. PV modeling

Photovoltaic panel is modeled by considering an association of N_{PP} strings in parallel. Each string is formed by N_{SS} modules in series. The module consists of N_S cells in series. One diode model of the PV module is widely used in the literature (Fig. 2). This model consists of a photonic current source I_{ph}, a junction diode D and a resistor R_p connected in parallel. The whole assembly is connected in series with a resistor R_s.

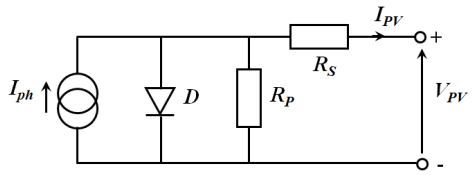

Figure 2. Model of PV module

Photovoltaic module delivers I_{PV} current and V_{PV} voltage at its output. The output current is expressed as follow:

$$I_{PV} = I_{ph} - I_0\left[\exp\left(\frac{V_{PV}+R_sI_{PV}}{N_SV_T\alpha}\right)-1\right]-\frac{V_{PV}+R_sI_{PV}}{R_P} \quad (1)$$

$$I_0 = \frac{I_{sc}+K_I\Delta_T}{\exp\left(\frac{V_{oc}+K_V\Delta_T}{N_S\alpha V_T}\right)-1} \quad (2)$$

$$I_{ph} = \left(I_{sc}+K_I\Delta_T\right)\frac{G}{G_n} \quad (3)$$

where, V_{oc} is the open-circuit voltage, I_{sc} is the short-circuit current, K_V is the open-circuit voltage/temperature coefficient,K_I is the short circuit current/temperature coefficient, V_T thermal voltage and α is the ideality factor.

B. DC/DC Converter Model

As shown in Fig. 3, the boost converter consist of an association of inductance L, capacitor C, diode D and an electronic switch designed by IGBT-Diode transistor. A pulse width modulation PWM signal controls the electronic switch.

Output voltage is expressed as:

$$V_{DC} = \frac{V_{PV}}{1-D} \quad (4)$$

where, V_{PV} and V_{DC} are respectively the input and output voltage. D is the duty cycle value located between 0 and 1.

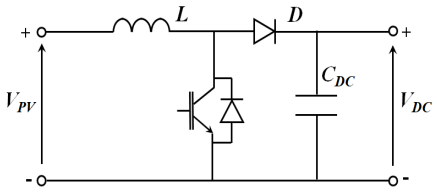

Figure 3. Boost converter model

C. DC/AC Converter Model

A two level inverter model is used in this paper as shown in Fig. 4. Each arm consists of two complementary switches modeled by an associated IGBT-Diode transistor.

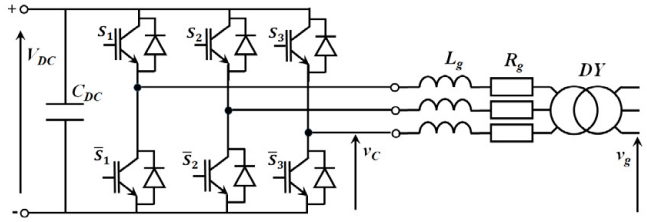

Figure 4. Inverter model

D. Filter and Transformer Design

A series resistance and inductance filter is connected to a DY transformer. Equivalent model in per unit for DY transformer in the positive sequence is described in Fig. 5,where: V_L and V_H denote low and high voltage respectively, z_1 and z_2 are the per-unit leakage complex impedance for primary and secondary winding refereed to the primary winding, G and B_m represent respectively losses resistances and magnetizing current. The DY transformer includes a 30° phase shift in the high winding voltage.

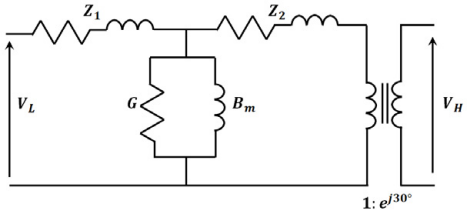

Figure 5. Per unit transformer model in positive sequence

Using Kirchhoff voltage law KVL for the filter associated to transformer (we assume that winding resistance and exciting current are neglected), voltage equations are given in per unit (time is kept in seconds) and in dq axis representation system (Park transformation) as:

$$\begin{cases} V_{cd} = V_{gd} + R_{Tot}I_{gd} + \frac{1}{\omega_b}L_{Tot}\frac{dI_{gd}}{dt} - L_{Tot}I_{gq} \\ V_{cq} = V_{gq} + R_{Tot}I_{gq} + \frac{1}{\omega_b}L_{Tot}\frac{dI_{gq}}{dt} + L_{Tot}I_{gd} \end{cases} \quad (5)$$

where:

- V_c and V_g (in dq-axis) are converter and grid voltage respectively and ω_b is the base angular speed;
- $\left(R_{Tot} = R_g + R_T \quad ; \quad L_{Tot} = L_g + L_T\right)$

- (R_T, L_T) represent the total resistances and inductances, in per unit, of the transformer windings referred to the low voltage.

E. DC Bus Voltage Mode

The power flow equations through the DC bus voltage are given as follows:

$$C_{DC}V_{DC}\frac{dV_{DC}}{dt}=P_{PV}-\frac{3}{2}V_{gd}I_{gd} \tag{6}$$

Equation (6) in per unit becomes:

$$C_{DC}V_{DC}\frac{dV_{DC}}{dt}=\frac{3}{2}\omega_b\left(P_{PV}-V_{gd}I_{gd}\right) \tag{7}$$

or in the linear form:

$$\frac{dw}{dt}=\frac{3}{C_{DC}}\omega_b\left(P_{PV}-V_{gd}I_{gd}\right) \tag{8}$$

where: P_{PV} is the photovoltaic power and $w=V_{DC}{}^2$.

We assume that losses power in the boost converter, inverter, filter and transformer are neglected.

IV. ADRC CONTROL

The ADRC structure is becoming more and more popular, several authors have been interested in its description and analysis [24], [26-28].

To illustrate its concept, we first consider the general model of an nth-order nonlinear time-varying (NLTV) dynamical system with a single input *u* and a single output *y* described by the following equation:

$$y(t)^{(n)}=f\left(y(t)^{(n-1)},y(t)^{(n-2)},\ldots,y(t),d(t)\right)+bu(t) \tag{9}$$

where:

- *d(t)* represents the external disturbances and *b* is a constant parameter;
- $f=f\left(y(t)^{(n-1)},y(t)^{(n-2)},\ldots,y(t),d(t)\right)$ represent the unknown NLTV dynamics of the system. It describes the totality of the disturbances, whether they are internal or external. We note that for this system, only the order and the parameter *b* are given.

Since the detailed mathematical system model is unknown, the ADRC provides an alternative way to control this kind of problem by estimating and rejecting in real time the totality of the perturbations *f*.

We denote by $\tilde{f}$ the estimate of the totality of disturbances. By choosing a control law in the form:

$$u=\frac{-\tilde{f}+u_0}{b} \tag{10}$$

With a well-tuned observer, the original NLTV system (9) is reduced to an equivalent cascaded integrator system which is easily controlled (where u_0 is the new control input signal):

$$y^{(n)}=f+b\frac{-\tilde{f}+u_0}{b}\approx u_0 \tag{11}$$

Nevertheless, such an approach is only justified if an estimation of perturbations is possible. This is the purpose and role of the extended state observer (ESO).

A. Extended State Observer

The ADRC relies on the proper operation of the ESO and its ability to establish a good estimate of perturbations. For this purpose, an extended state vector is constructed with an additional state, namely the function *f* assumed to be differentiable and defined as follows:

$$X=\begin{bmatrix}x_1 & x_2 & \ldots & x_n & x_{n+1}\end{bmatrix}^t=\begin{bmatrix}y & \dot{y} & \ldots & y^{(n-1)} & f\end{bmatrix}^t \tag{12}$$

Equation (9) is written as:

$$\begin{cases}\dot{x}_1=x_2\\ \vdots\\ \dot{x}_n=x_{n+1}+bu\\ \dot{x}_{n+1}=h;\ h=\dot{f}\\ y=x_1\end{cases} \tag{13}$$

or in matrix form:

$$\dot{X}=AX+Bu+Eh \tag{14}$$

where:

$$A=\begin{bmatrix}0 & 1 & \cdots & 0\\ \vdots & & \ddots & \vdots\\ 0 & 0 & \cdots & 1\\ 0 & 0 & \cdots & 0\end{bmatrix}_{(n+1)\times(n+1)}\quad B=\begin{bmatrix}0\\ \vdots\\ b\\ 0\end{bmatrix}_{(n+1)\times 1}\quad E=\begin{bmatrix}0\\ \vdots\\ 0\\ 1\end{bmatrix}_{(n+1)\times 1}$$

The extended state observer ESO is then constructed for (14) as:

$$\begin{cases}\dot{Z}=AZ+Bu+G\left(y-\tilde{y}\right)\\ \tilde{y}=CZ\end{cases} \tag{15}$$

where:

$$\begin{cases}Z=\begin{bmatrix}z_1 & z_2 & \cdots & z_{n+1}\end{bmatrix}^t\\ G=\begin{bmatrix}g_1 & g_2 & \cdots & g_{n+1}\end{bmatrix}^t\\ C=\begin{bmatrix}1 & 0 & \cdots & 0\end{bmatrix}\end{cases}$$

In its original form, as reported in [29-30], the functions g_i with *(i=1...n+1)* are non-linear functions. To facilitate its construction and the determination of its parameters, Z. Gao proposed to replace the functions by constant gains [31], i.e.:

$$G=\begin{bmatrix}g_1 & g_2 & \cdots & g_{n+1}\end{bmatrix}=\begin{bmatrix}\omega_0\beta_1 & \omega_0{}^2\beta_2 & \cdots & \omega_0{}^{n+1}\beta_{n+1}\end{bmatrix} \tag{16}$$

The pole placement technique is adopted to set gains so that $\left(s^{n+1}+\beta_1 s^n+\ldots+\beta_n s+\beta_{n+1}\right)$ is Hurwitz. To simplify the setting, β_i are chosen to have:

$$s^{n+1}+\beta_1 s^n+\ldots+\beta_n s+\beta_{n+1}=(s+1)^{n+1} \tag{17}$$

where:

$$\beta_i=\frac{(n+1)!}{i!(n+1-i)!}\qquad i=1,2..n+1 \tag{18}$$

The characteristic polynomial of (15) then becomes:

$$\lambda(s)=\left|sI-\left(A-GC\right)\right|=\left(s+\omega_0\right)^n \tag{19}$$

This reduces the ESO setting to a single parameter ω_0.

B. Control Low

The control law *u* allows the system to be reduced to a cascade of integrators, which can be controlled by a generalized PD controller. We define:

$$r=\left[y_r,\dot{y}_r,\ldots,y_r^{(n-1)}\right]=\left[r_1,r_2,\ldots,r_n\right] \tag{20}$$

where:

- r_1 denotes the input bounded reference signal, which the output should follow according to the control law;
- r_i its *(i-1)*th derivative for *i = 2...n*.

We then write:

$$u_0=\sum_{i=1}^{n}g_i\left(r_i-z_i\right) \tag{21}$$

where:g_i are non-linear functions.

NB: in linear form, functions g_i *are replaced by constants coefficients* k_i.

We define:

$$\begin{cases} e_i = r_i - x_i & (i = 1..n) \\ \tilde{x}_i = x_i - z_i & (i = 1..n+1) \end{cases} \tag{22}$$

The state equation for the dynamic error is written as:

$$\dot{e} = Ae + B\tilde{x} \tag{23}$$

where:

$$A = \begin{bmatrix} 0 & 1 & 0 & \cdots & 0 \\ \vdots & \ddots & \ddots & \ddots & \vdots \\ 0 & \cdots & 0 & 1 & 0 \\ -k_1 & \cdots & -k_{n-2} & -k_{n-1} & -k_n \end{bmatrix}_{n\times n}$$

$$B = \begin{bmatrix} 0 & \cdots & 0 & 0 \\ \vdots & \ddots & \vdots & \vdots \\ 0 & \cdots & 0 & 0 \\ -k_1 & \cdots & -k_n & -1 \end{bmatrix}_{n\times(n+1)}$$

$$e = \begin{bmatrix} e_1 \\ \vdots \\ e_n \end{bmatrix}_{n\times 1} \quad ; \quad \tilde{x} = \begin{bmatrix} \tilde{x}_1 \\ \vdots \\ \tilde{x}_{n+1} \end{bmatrix}_{(n+1)\times 1}$$

The k_i terms are chosen so that the polynomial $(s^n + k_n s^{n-1} + \ldots + k_1)$ is of type Hurwitz. As before, to simplify the design of the controller, we take:

$$s^n + k_n s^{n-1} + \ldots + k_1 = (s + \omega_c)^n \tag{24}$$

where:

$$k_i = \frac{n!}{(i-1)!(n+1-i)!}\omega_c^{n+1-i} \tag{25}$$

and $\omega_c > 0$ represents the controller bandwidth, which make the closed loop characteristic polynomial to have n poles at $-\omega_c$.

In practice, ω_0 is often chosen in the range of $3\sim7\omega_c$, which allows to simplify the tuning of the linear ADRC to a single parameter ω_c.

For the first order system (n=1):

- The ESO setting is:

$$Z = \begin{pmatrix} z_1 \\ z_2 \end{pmatrix}; \quad \begin{pmatrix} \beta_1 \\ \beta_2 \end{pmatrix} = \begin{pmatrix} 2 \\ 1 \end{pmatrix}; \quad \begin{pmatrix} g_1 \\ g_2 \end{pmatrix} = \begin{pmatrix} \beta_1\omega_0 \\ \beta_2\omega_0^2 \end{pmatrix} = \begin{pmatrix} 2\omega_0 \\ \omega_0^2 \end{pmatrix}$$

- The control low setting is:

$$\begin{cases} r = [y_r] \quad ; \quad k_1 = \omega_c \, ; \quad u_0 = k_1(y_r - z_1) \\ \tilde{f} = z_2 \quad ; \quad u = \dfrac{u_0 - \tilde{f}}{b_0} = \dfrac{u_0 - z_2}{b_0} \end{cases}$$

ADRC schematic diagram is illustrated in Fig. 6.

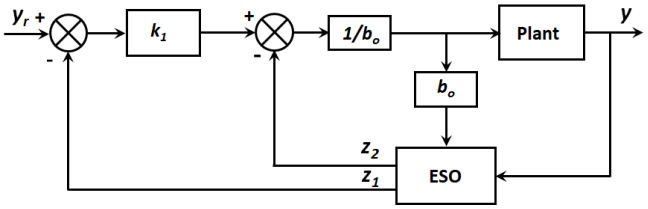

Figure 6. A first order system ADRC structure

V. Inverter Control

The DC/AC inverter can supply 250 KW to a three-phase load connected to the grid. Depending on the weather conditions, the load will be supplied totally or partially by the PV generator. In case of low photovoltaic production, the missing energy will be taken from the grid.

In order to control the DC/AC converter, two cascaded loops are used. The slower one controls the DC bus voltage V_{DC}. The other, faster one, controls direct and quadratic currents (I_d&I_q) flowing through the RL filter.

A. Current Control (Intern Loop)

Equation (5) of the filter associated to the transformer is written in ADRC canonical form as:

$$\begin{cases} \dfrac{dI_{gd}}{dt} = f_d(I_{gd}, d, t) + b_{o\_d}u_d \\ \dfrac{dI_{gq}}{dt} = f_q(I_{gq}, d, t) + b_{o\_q}u_q \end{cases} \tag{26}$$

where:

$$f_d(I_{gd}, d, t) = \frac{\omega_b}{L_{Tot}}\left(-V_{gd} - R_{Tot}I_{gd} + L_{Tot}I_{gq}\right) + \left(\frac{\omega_b}{L_{Tot}} - b_{o\_d}\right)V_{cd}$$

$$f_q(I_{gq}, d, t) = \frac{\omega_b}{L_{Tot}}\left(-V_{gq} - R_{Tot}I_{gq} - L_{Tot}I_{gd}\right) + \left(\frac{\omega_b}{L_{Tot}} - b_{o\_q}\right)V_{cq}$$

- $u_d = V_{cd}$ and $u_q = V_{cq}$
- b_{o_d} and b_{o_q} are two parameters to estimate and they are typically chosen equal. A first approximation might be: $b_{o\_d} = b_{o\_q} \approx \dfrac{\omega_b}{L_{Tot}}$

Note:

- Quadratic current reference I_{q_ref} is set to be zero, thus only active power is flowing through filter and reactive power is null.
- Direct current reference I_{d_ref} is generated by the DC voltage controller.
- The shift angle induced by DY transformer will be take into account to evaluate the reference value U_{abc_ref} used for the inverter PWM block to generate the appropriates IGBTs-Diodes switching signals (Fig. 8).

B. DC Bus Voltage Control

Equation (8) can be writing into ADRC canonical form as:

$$\begin{cases} \dfrac{dw}{dt} = f_w(w, d, t) + b_{w\_0}u_w \\ u_w = I_{gd} \end{cases} \tag{27}$$

where:

- $f_w(w, d, t) = \dfrac{3}{C_{DC}}\omega_b\left(P_{PV} - V_{gd}I_{gd}\right) - b_{w\_0}I_{gd}$
- b_{w_0} is the parameter to estimate.

Fig. 8 represents the schematic control diagram applied to the inverter.

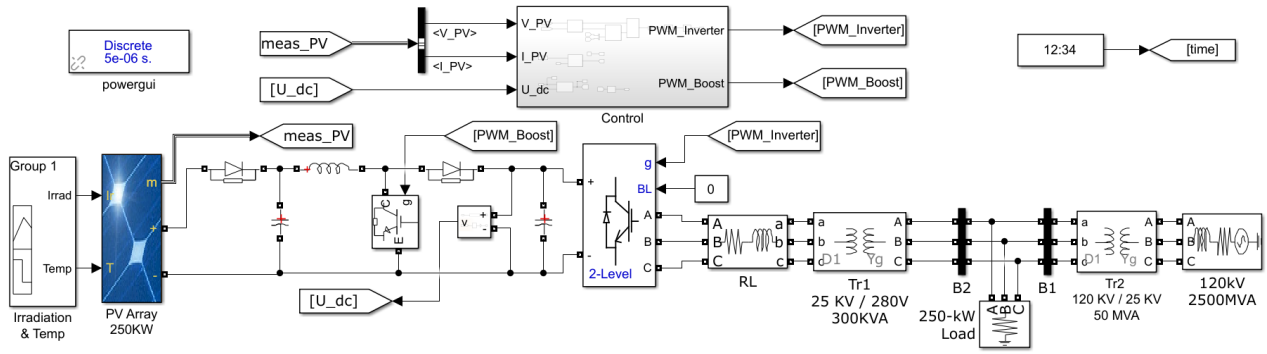

Figure 7. Simulation system model

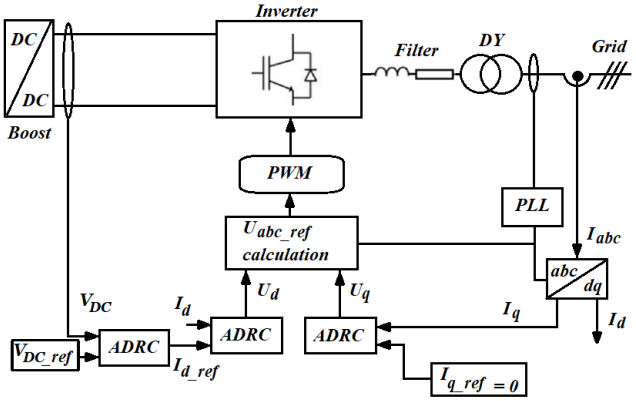

Figure 8. Inverter control schematic diagram

VI. Boost Control

The DC/DC converter is controlled to extract the maximum power from the PV array for each condition such as atmospheric changes (irradiation and temperature) or load variations. In this work, two techniques are investigated, the ADRC control based on the incremental conductance ADRC_IncCond and a fuzzy logic control FLC, which will be compared to the classical perturb and observe P&O control.

A. ADRC_IncCond for MPPT Control

The output PV power is $P_{PV}=V_{PV} \times I_{PV}$, where I_{PV} and V_{PV} are PV array output current and voltage respectively.

At the maximum power point MPP we have:

$$\frac{dP_{PV}}{dV_{PV}} = I_{PV} + V_{PV}\frac{dI_{PV}}{dV_{PV}} = 0 \tag{28}$$

Considering the time derivatives of the voltage and current, the error e can be written as follows:

$$e = I_{PV} + V_{PV}\frac{\frac{\partial I_{PV}}{\partial t}}{\frac{\partial V_{PV}}{\partial t}} \tag{29}$$

The main objective is to keep the error e at zero to achieve a MPP tracking. Since the ADRC does not require detailed knowledge of the system, a first order model will be adopted as a first approximation.

$$\frac{de}{dt} = f(e,d,t) + b_o u \tag{30}$$

where: $u = D$ (D duty cycle) and b_0 a parameter to estimate.

Fig. 9 shows Simulink diagram control of MMPT based on ADRC_IncCond technique.

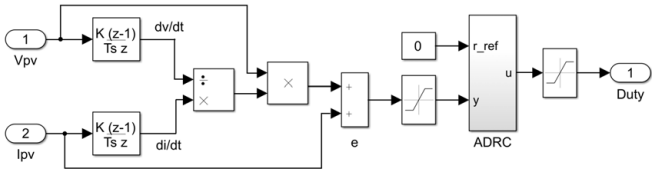

Figure 9. ADRC_IncCond MPPT Simulink model

B. FLC MPPT technique

Fuzzy logic controllers are widely used in several industrial applications, and moreover, this type of controller does not require detailed knowledge of the model. It based on three blocks: Fuzzification, rule base table operation, and Defuzzification. The input variables are converted into linguistic variables used by the membership functions. For MPPT control, the input variables typically used are:

- Error E

$$E = \frac{\Delta P_{PV}}{\Delta V_{PV}} = \frac{P_{PV}(k) - P_{PV}(k-1)}{V_{PV}(k) - V_{PV}(k-1)} \tag{31}$$

- Change of error CE

$$CE = E(k) - E(k-1) \tag{32}$$

Error E checks for the MPP while change of error CE indicates the direction of voltage change. The output variable is ratio change in duty cycle dD used for DC/DC converter.

Membership functions and fuzzy rules for input and output variables are listed respectively in Fig. 10 and Table I.

The three strategies for controlling the maximum power point MPP will be evaluated in Matlab Simulink according to the schematic diagram (Fig. 11) with consideration of their efficiency η defined as:

$$\eta = \frac{P_{PV}}{P_{MP}} \tag{33}$$

where: P_{PV} and P_{MP} are respectively power extracted from PV and theoretical maximum power.

Table I. Fuzzy Logic Rules

E	CE						
	NB	**NM**	**NS**	**ZE**	**PS**	**PM**	**PB**
NB	NB	NB	NB	NB	NM	NS	ZE
NM	NB	NB	NB	NM	NS	ZE	PS
NS	NB	NB	NM	NS	ZE	PS	PM
ZE	NB	NM	NS	ZE	PS	PM	PB
PS	NM	NS	ZE	PS	PM	PB	PB
PM	NS	ZE	PS	PM	PB	PB	PB
PB	ZE	PS	PM	PB	PB	PB	PB

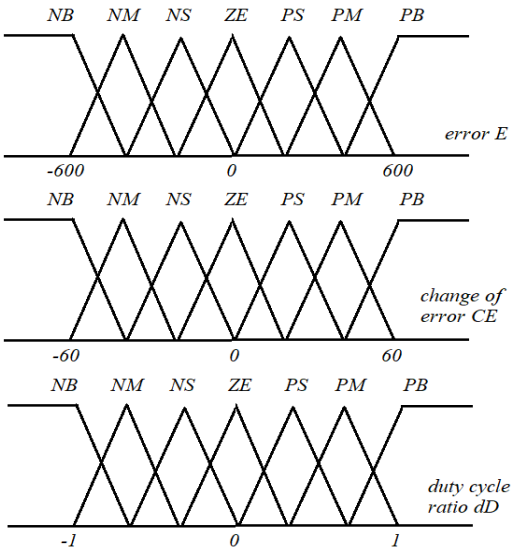

Figure 10. FLC input and output variables

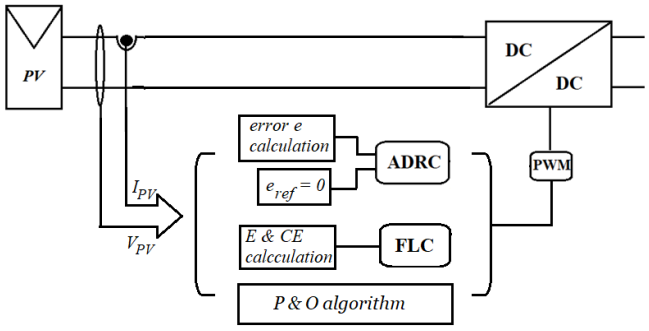

Figure 11. Overview of the MPPT schematic diagram

VII. Discuss and Results

The performance of the proposed control was tested by simulations under Matlab simulink software. The grid-connected photovoltaic system consists of 135 strings of 5 modules in series to cut 250 KW. The characteristics of the PV array are listed in Table II.

The simulation model for the whole system is shown in Fig. 7, which is used to check out the performance of the proposed control strategies.

Three control schemes are applied to the boost converter to track the maximum power point MPP under atmospheric variations. We first applied the ADRC_IC control, then FLC and finally the classical P&O algorithm. While the converter was kept under control, for all three strategies, using the ADRC control for both the external loop (DC bus voltage) and internal loop (direct and quadratic currents in dq-axis reference).

PV system and control parameters used in the simulations are listed respectively in Table III and Table IV.

To evaluate the effectiveness of the control, the system is subjected to a step change in irradiance from 1000 W/m^2 to 800 W/m^2 at time *t=0.4s*. A second step change is applied from 800 W/m^2 to 1000 W/m^2 at time *t=1.2s*.

The temperature is also varied from 25 °C to 45 °C at time *t=0.8s*, followed by a variation from 45 °C to 25 °C at time *t=1.6s* (Fig. 12).

As shown in Fig. 13, maximum power is extract from PV array for the three MPPT strategies (254 KW in standard test conditions 1000 W/m^2 and 25°C). By zooming in on the power curves at step change (Fig. 13), we concluded that ADRC_IncCond and FLC have a better dynamic performance than P&O (faster response and no overshoot). In terms of quality, the PV power produced by the ADRC_IncCond control is very stable and shows few oscillations compared to the FLC and P&O controls. The latter shows more oscillations due to the classical algorithm used.

Table V shows the efficiency of the control strategies under standard test conditions, taking into account the magnified curves described in Fig. 13. It can be seen that ADRC_IncCond performs well compared to the other two controls.

As shown in Fig. 14, the DC bus voltage is kept constant and overshoots are less than 5% (less than 30V) even if external disturbances occur.

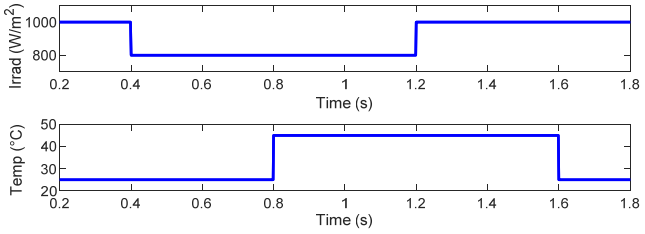

Figure 12. Temperature and irradiation variations

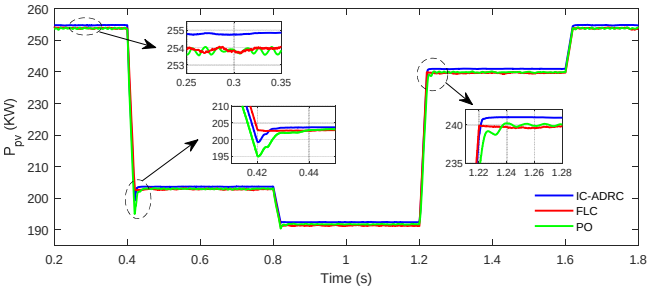

Figure 13. Output PV power

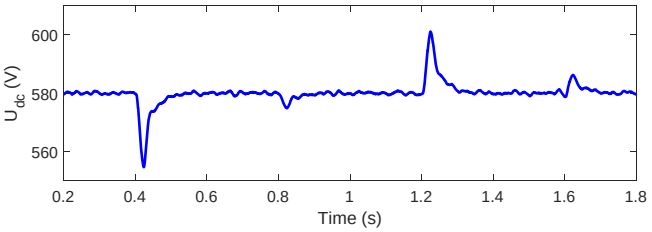

Figure 14. DC bus voltage

It should be noted, as discussed in previous studies [23-24], that ADRC is one of the most robust control methods. It is able to provide good control even if the system is subject to variations in its internal or external parameters. Indeed, its design does not require exact knowledge of the system.

The current waveform at bus 2 is practically sinusoidal and has a zero phase shift with respect to the voltage at the output of the transformer (Fig. 15 and Fig.16), which means that no reactive power flow is exchanged with the grid, as expected by the inverter control (Fig. 17).

The powers in buses 1 and 2 are presented in Fig. 17, it can be seen that the 250 KW load absorbs all the energy it needs from the PV generator as long as the standard conditions are met (1000 W/m^2 and 25°C). If this is not the case, the energy deficit is supplied by the grid. Similarly, if there is no load or if the load is less than 250 KW, the PV array injects the excess energy directly into the grid.

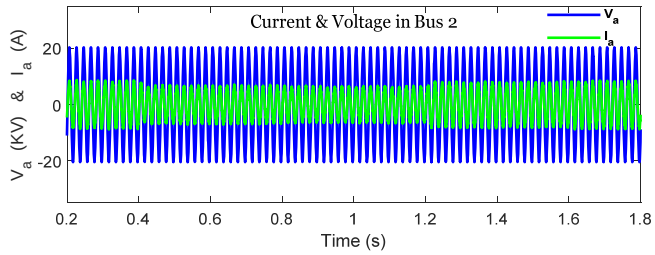

Figure 15. Current and voltage in bus 2

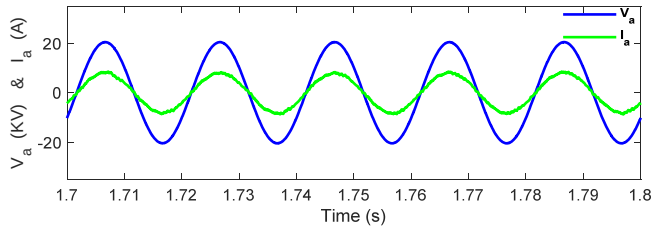

Figure 16. Zoom of current and voltage in bus 2

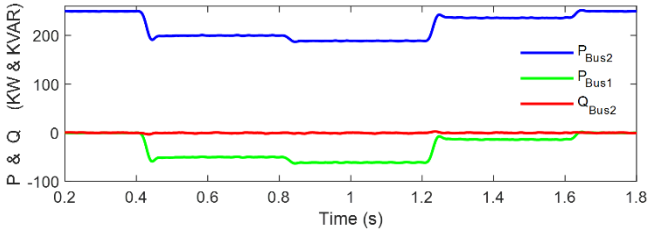

Figure 17. Active and reactive powers in buses 1 & 2

TABLE II. PV ARRAY CHARACTERISTICS

Parameter	Value
Maximum output power P_{MAX}	414.801 W
Open circuit voltage V_{OC}	85.3 V
short-circuit current I_{SC}	6.09 A
Voltage at maximum power point V_{MP}	72.9 V
Current at maximum power point I_{MP}	5.69 A
Number of cells in series N_S	128
Number of modules in series per string	5
Number of parallel string	123

TABLE III. PV SYSTEM PARAMETERS

Parameter	Value
Boost converter	C_{PV} = 1.7 mF ; C_{DC} = 17 mF ; L_{BOOST} = 1 mH
	V_{DC} = 580V ; PWM = 5 KHz
Filter	R_g = 1.5 mΩ ; L_g = 1 mH
Transformer	T_1 : (300 KVA – 280V / 25 KV- ΔY)
	T_2 : (50 MVA – 25 KV / 120 KV- YΔ)
Simulink solver	Ode23t – Step size 5µs

TABLE IV. ADRC CONTROL PARAMETERS

Parameter	Value
MPPT	b_o = 1000 ; k_1 = 350 ; ω_o = 1750
DC bus voltage	b_o = -580 ; k_1 = 50 ; ω_o = 150
Current loop	b_o = 561 ; k_1 = 500 ; ω_o = 2500

TABLE V. THE EFFICIENCY OF MPP TRACKING CONTROLS

Standard test conditions	ADRC_IncCond	FLC	P&O
1000 W / m^2, 25°C	99.88 %	99.52 %	99.48 %

VIII. CONCLUSION

In this paper, a model of a two-stage grid-connected photovoltaic system is developed. The model is subjected to varying atmospheric conditions in order to highlight the performance of the controllers used. An active disturbance rejection control is presented and applied to control the whole system.

The performance and robustness of the ADRC is examined under disturbances for MPPT and inverter control, using the extended state observer which estimates the overall uncertainties in real time, since the detailed mathematical model is not required.

MMPT techniques for photovoltaic arrays are analyzed and evaluated. The simulation results showed the good performance of ADRC_IncCond compared to FLC and P&O in terms of efficiency, response time and stability.

REFERENCES

[1] G. Carrington, J. Stephenson, "The politics of energy scenarios: are international energy agency and other conservative projections hampering the renewable energy transition?," Energy research & social science, vol. 46, pp. 103-113, 2018. doi:10.1016/j.erss.2018.07.011

[2] E. Asmelash, G. Prakash, R. Gorini, D. Gielen, "Role of IRENA for global transition to 100% renewable energy," In: Uyar T. (eds) Accelerating the Transition to a 100% Renewable Energy Era. Lecture Notes in Energy, vol. 74, pp. 51-71, 2020, Springer, Cham. doi:10.1007/978-3-030-40738-4_2

[3] H. Bevrani, A. Ghosh, G. Ledwich, "Renewable energy sources and frequency regulation: survey and new perspectives," IET Renewable Power Generation, vol. 4, no. 5, pp. 438, 2010. doi:10.1049/iet-rpg.2009.0049

[4] E. Jahan et al., "Primary frequency regulation of the hybrid power system by deloaded PMSG-based offshore wind farm using centralised droop controller," The Journal of Engineering, vol. 2019, no. 18, pp. 4950-4954, 2019. doi:10.1049/joe.2018.9326

[5] F. J. Lin, K. C. Lu, B. H. Yang, "Recurrent fuzzy cerebellar model articulation neural network based power control of a single-stage three-phase grid-connected photovoltaic system during grid faults," IEEE Transactions on Industrial Electronics, vol. 64, no. 2, pp. 1258–1268, 2017. doi:10.1109/tie.2016.2618882

[6] A. B. Rey-Boué, N. F. Guerrero-Rodríguez, J. Stöckl, T. I. Strasser, "Modeling and design of the vector control for a three-phase single-stage grid-connected PV system with LVRT capability according to the Spanish grid code," Energies, vol. 12, no. 15, pp. 2899, 2019. doi:10.3390/en12152899

[7] N. Aouchiche, "Meta-heuristic optimization algorithms based direct current and DC link voltage controllers for three-phase grid connected photovoltaic inverter," Solar Energy, vol. 207, pp. 683–692, 2020. doi:10.1016/j.solener.2020.06.086

[8] T. Selmi, M. Abdul-Niby, L. Devis, A. Davis, "P&O MPPT implementation using MATLAB/Simulink," Ninth International Conference on Ecological Vehicles and Renewable Energies (EVER) IEEE, pp. 1-7, 2014. doi:10.1109/ever.2014.6844065

[9] E. Mamarelis, G. Petrone, G. Spagnuolo, "A two-steps algorithm improving the P&O steady state MPPT efficiency," Applied Energy, vol. 113, pp. 414-421, 2014. doi:10.1016/j.apenergy.2013.07.022

[10] F. Liu, Y. Kang, Y. Zhang, S. Duan, "Comparison of P&O and hill climbing MPPT methods for grid-connected PV converter," In 2008 3rd IEEE Conference on Industrial Electronics and Applications, pp. 804-807, June 2008. doi:10.1109/ICIEA.2008.4582626.

[11] S. Z. Mirbagheri, S. Mekhilef, S. M. Mirhassani, "MPPT with Inc.Cond method using conventional interleaved boost converter," Energy Procedia, vol. 42, pp. 24-32, 2013. doi:10.1016/j.egypro.2013.11.002

[12] K. Ishaque, Z. Salam, G. Lauss, "The performance of perturb and observe and incremental conductance maximum power point tracking method under dynamic weather conditions," Applied Energy, vol. 119, pp. 228-236, 2014. doi:10.1016/j.apenergy.2013.12.054

[13] C. H. Lin, C. H. Huang, Y. C. Du, J. L. Chen, "Maximum photovoltaic power tracking for the PV array using the fractional-order incremental conductance method," Applied Energy, vol. 88, no. 12, pp. 4840-4847, 2011. doi:10.1016/j.apenergy.2011.06.024

[14] A. Safari, S. Mekhilef, "Simulation and hardware implementation of incremental conductance MPPT with direct control method using cuk converter," IEEE Transactions on Industrial Electronics, vol. 58, no. 4, pp. 1154-1161, 2011. doi:10.1109/tie.2010.2048834

[15] H. Bounechba, A. Bouzid, K. Nabti, H. Benalla, "Comparison of perturb & observe and fuzzy logic in maximum power point tracker for PV systems," Energy Procedia, vol. 50, pp. 677-684, 2014. doi:10.1016/j.egypro.2014.06.083

[16] A. M. Noman, K. E. Addoweesh, H. M. Mashaly, "A fuzzy logic control method for MPPT of PV systems," IECON 2012 - 38th Annual Conference on IEEE Industrial Electronics Society, pp. 874-880. doi:10.1109/iecon.2012.6389174

[17] B. Bendib, F. Krim, H. Belmili, M. F. Almi, S. Boulouma, "Advanced fuzzy MPPT controller for a stand-alone PV system," Energy Procedia, vol. 50, pp. 383-392, 2014. doi:10.1016/j.egypro.2014.06.046

[18] H. Rezk, A. M. Eltamaly, "A comprehensive comparison of different MPPT techniques for photovoltaic systems," Solar Energy, vol. 112, pp. 1-11, 2015. doi:10.1016/j.solener.2014.11.010

[19] A. K. Rai, N. D. Kaushika, B. Singh, N. Agarwal, "Simulation model of ANN based maximum power point tracking controller for solar PV system," Solar Energy Materials and Solar Cells, vol. 95, no. 2, pp. 773-778, 2011. doi:10.1016/j.solmat.2010.10.022

[20] S. Messalti, A. Harrag, A. Loukriz, "A new variable step size neural networks MPPT controller: review, simulation and hardware implementation," Renewable and Sustainable Energy Reviews, vol. 68, pp. 221-233, 2017. doi:10.1016/j.rser.2016.09.131

[21] A. Boualouch, A. Essadki, T. Nasser, A. Boukhriss, A. Frigui, "Power control of DFIG in WECS using backstipping and sliding mode controller," International Journal of Electrical and Computer Engineering, 2015, vol. 9, no 6, p. 612-618, 2015. doi.org/10.5281/zenodo.1108312

[22] Y. Errami, M. Ouassaid, M. Cherkaoui, M. Maaroufi, "Sliding mode control scheme of variable speed wind energy conversion system based on the PMSG for utility network connection," Studies in Computational Intelligence, pp. 167-200, 2014. doi:10.1007/978-3-319-11173-5_6

[23] A. Boukhriss, A. Essadki, A. Bouallouch, T. Nasser, "Maximization of generated power from wind energy conversion systems using a doubly fed induction generator with active disturbance rejection control," Second World Conference on Complex Systems (WCCS), pp. 330-335, 2014. doi:10.1109/ICoCS.2014.7060907

[24] A. Boukhriss, T. Nasser, A. Essadki, A. Boualouch, "Active disturbance rejection control for DFIG based wind farms under unbalanced grid voltage," International Review on Modelling and Simulations (IREMOS), vol. 7, no. 1, pp. 95-105, 2014. doi:10.15866/iremos.v7i1.265

[25] A. Boualouch, A. Essadki, T. Nasser, A. Frigui, A. Boukhriss, "ADRC performance in power control of DFIG used in wind turbine during grid voltage fault," International Journal of Control and Automation, vol. 11, no. 9, pp. 43–56, 2018. doi:10.14257/ijca.2018.11.9.05

[26] Q. Zheng, L. Q. Gaol, Z. Gao, "On stability analysis of active disturbance rejection control for nonlinear time-varying plants with unknown dynamics," Proceedings of the 46th IEEE Conference on Decision and Control, 2007, pp. 3501-3506. doi:10.1109/CDC.2007.4434676

[27] S. Shao, Z. Gao, "On the conditions of exponential stability in active disturbance rejection control based on singular perturbation analysis," International Journal of Control, vol. 90, no. 10, pp. 2085-2097, 2017. doi:10.1080/00207179.2016.1236217

[28] B. Z. Guo, Z. L. Zhao, "On convergence of non-linear extended state observer for multi-input multi-output systems with uncertainty," IET Control Theory & Applications, vol. 6, no. 15, pp. 2375–2386, 2012. doi:10.1049/iet-cta.2012.0123

[29] Z. Gao, Y. Huang, J. Han, "An alternative paradigm for control system design," Proceedings of the 40th IEEE Conference on Decision and Control (Cat. No.01CH37228), pp. 4578-4585 vol.5, 2001. doi:10.1109/CDC.2001.980926

[30] J. Han, "From PID to active disturbance rejection control," in IEEE Transactions on Industrial Electronics, vol. 56, no. 3, pp. 900-906, March 2009, doi:10.1109/TIE.2008.2011621

[31] Z. Gao, "Scaling and bandwidth-parameterization based controller tuning," Proceedings of the 2003 American Control Conference, pp. 4989-4996, 2003, doi:10.1109/ACC.2003.1242516